ACS APPLIED MATERIALS & INTERFACES

Research Article

www.acsami.org

Crystallization under One-Dimensional Confinement in Alumina Nanopores of Poly(trimethylene terephthalate) and Its Composites with Single Wall Carbon Nanotubes

Ignacio Martín-Fabiani,*[,†] Mari-Cruz García-Gutiérrez,[†] Daniel R. Rueda,[†] Amelia Linares,[†] Jaime J. Hernández,[‡] Tiberio A. Ezquerra,[†] and Michael Reynolds[§]

[†]Instituto de Estructura de la Materia (IEM-CSIC), Serrano 121, 28006 Madrid, Spain

[‡]Institut de Sciences de Matériaux de Mulhouse, 15 rue Jean Starcky, Mulhouse 68057, France

[§]ESRF, B.P. 220, F-38043 Grenoble Cedex, France

ABSTRACT: We report the preparation of semicrystalline polymer nanorods of PTT and of its nanocomposites with SWCNTs by infiltration of the molten polymer into disordered anodic alumina membranes. An accurate study of the crystalline orientation of these systems has been accomplished by means of X-ray microdiffraction. While polymer residual film exhibits isotropic character, edge-on lamellae are formed upon approaching the polymer/membrane interface. This effect might be due to the elongational flow that takes place in the molten state as polymer chains infiltrate the AAO membrane. At the interface, edge-on and flat-on crystalline lamellae coexist as a consequence of the strong interaction between the polymer and the AAO surface. Inside the nanopores, the confined environment induces a kinetic selection of polymer crystals which only allows the growth of crystalline lamellae with its *a*-axis parallel to that of the pore. In the case of PTT/SWCNT nanocomposites, this effect, in conjunction with the strong interaction between polymer and AAO surface, seems to prevail over the templating effect of the carbon nanotubes and a similar orientation to that of the neat PTT case is observed.

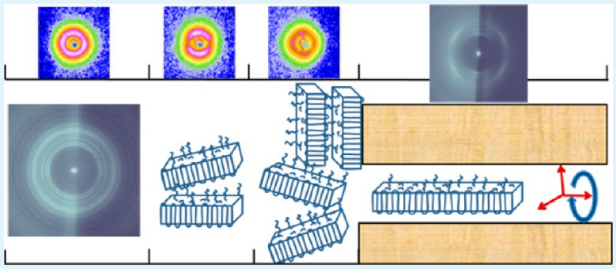

KEYWORDS: *polymer crystallization, melt wetting, confinement, nanocomposites, synchrotron radiation, poly(trimethylene terephthalate)*

1. INTRODUCTION

One-dimensional confinement by nanoporous anodic aluminum oxide (AAO) templates is a common approach to preparing high aspect ratio nanostructures.[1] What makes this feasible is the wettability of high-surface-energy solids like AAO with low-surface-energy liquids,[2] including polymer melts. Most of the studies have focused on the use of ordered AAO membranes, first developed by Masuda performing a double anodization process.[3] Nonetheless, several works have been published using disordered AAO membranes, showing that interesting confinement effects may arise when using these templates.[4,5] Depending on different factors such as annealing temperature, pore size, and spreading coefficient of the AAO/polymer system, partial or total wetting is achieved.[5] Under these conditions of restricted geometry and strong interaction with the pore wall, polymer crystallization takes place in a different way when compared to the bulk material. In fact, it has been shown that spherulitic growth can be suppressed under one-dimensional confinement, giving rise to previously unseen crystallization phenomena.[4,6−8] Moreover, the possibility to build arrays of polymer nanorods opens up new perspectives in fields such as photovoltaics.[9]

Poly(trimethylene terephthalate) (PTT) is a semicrystalline aromatic polyester which has attracted the interest of the textile market since the discovery of a new and cheaper synthesis route.[10] Its outstanding mechanical and optical properties make it an attractive material for the fiber industry[11] as well as for optoelectronic[12] and nanophotonic[13,14] applications. PTT has already shown interesting features when nanostructured by several different methods such as laser induced periodic surface structuration (LIPSS)[15] and nanoimprint lithography (NIL).[16]

Polymer−single wall carbon nanotube (SWCNT) composites have been extensively studied due to their improved properties, having an enormous impact as materials for engineering.[17] The presence of SWCNTs in the polymer matrix has a strong impact on its crystallization, acting as templates[18] and leading to the formation of hybrid shish-kebab structures.[19] Spatial confinement of these nanocomposites seems to be an interesting topic, but apart from some work on composite thin films,[20] one-dimensional confinement has been scarcely studied[21] and nothing has been published yet, to our knowledge, on crystal orientation under these confinement conditions.

Received: April 5, 2013
Accepted: May 17, 2013
Published: May 17, 2013

In this work, we have investigated the impact of AAO and SWCNTs as templates for polymer crystallization under one-dimensional confinement in order to elucidate which one prevails when both are present.

2. EXPERIMENTAL SECTION

2.1. Materials and Sample Preparation. PTT was synthesized by polycondensation as previously described,[22] yielding a molecular weight of M_n = 31 294 g/mol and a polydispersity of M_w/M_n = 2.22, as determined by size exclusion chromatography (SEC). PTT is a semicrystalline polymer, with a melting temperature of T_m = 229 °C, which can be quenched from the molten state to render a fully amorphous state with a glass transition temperature of T_g = 44 °C, as determined by calorimetry. PTT pellets were melt pressed at 255 °C for 2 min under 5 bar pressure and 2 min under 15 bar pressure. The resulting films (200 μm thick) were quenched in ice cold water.

Nanocomposites of PTT and oxidized single-wall carbon nanotubes (CNI Technology Co., Texas, USA, synthesized using the HiPco method) were prepared by in situ polymerization.[22] The diameter of the SWCNTs, as characterized by Raman spectroscopy, ranges from about 0.6 to 1.4 nm.[23] A SWCNT weight concentration of 0.5% was chosen because it is the highest achievable by this method using SWCNT and PTT as a matrix.

Disordered anodic aluminum oxide (AAO) membranes[5] were purchased from Whatman Inc. in the form of disks 13 mm wide and 60 μm thick. They are used for filtering purposes, consisting of a thin, size-selective layer with a nominal pore diameter of 20 nm on top of a thick support layer with an average pore diameter of 200 nm. Membranes were immersed into hexane and sonicated for cleaning. AAO membranes, characterized by scanning electron microscopy (SEM), present an average pore diameter of about 25 nm (Figure 1a)

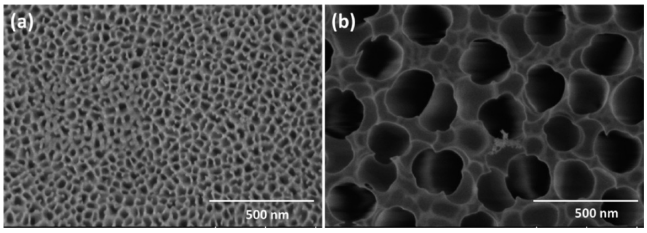

Figure 1. SEM images of disordered AAO membrane. (a) Upper side: The average pore diameter is around 25 nm. (b) Bottom side: The average pore diameter is around 200 nm.

on the upper side, which increases with pore depth reaching up to approximately 200 nm at the bottom of the membrane (Figure 1b). Infiltration was carried out by placing a 200 μm film of either PTT or PTT/SWCNT on top of the AAO membrane at 253 °C for 1 h, under nitrogen flow to prevent degradation. Upon melting, material infiltrated the pores of the membrane. The sample was then cooled at 3 °C/min until it reached room temperature.

2.2. Characterization and Data Analysis. Scanning electron microscopy (SEM) was carried out by means of a Hitachi S-8000, working at 0.5 kV to minimize sample damage. Images of combined secondary and backscattered electrons were acquired for the polymer nanorods.

Raman spectroscopy experiments were performed by using a Renishaw Raman InVia Reflex spectrophotometer, with excitation at 785 nm (diode laser) and a resolution of 2 cm^{-1}.

X-ray microdiffraction (μ-XRD) experiments were performed at the microfocus beamline (ID13) of the European Synchrotron Radiation Facility (ESRF). A wavelength of 0.09951 nm and a beam of 1 μm in diameter were used. Step scans (1 μm resolution) along the cross section of the sample and parallel to the main axis of the nanopores were accomplished, from the bulk sample outside the membrane to the infiltrated sample inside the membrane. The sample was mounted vertically with the nanopore axis carefully aligned perpendicular to the X-ray beam (Figure 2). Scattered intensity was recorded by a FReLoN detector (51.47 × 50.7 μm^2 pixel size; 16-bit readout) and analyzed

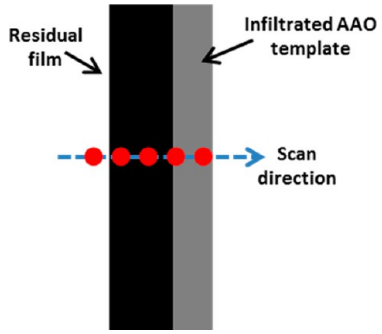

Figure 2. Schematic view of a μ-XRD experiment. The main axis of the membrane pores is aligned perpendicular to the X-ray beam (red dots). The average pore diameter of the disordered AAO template is around 25 nm at the interface with the polymer residual film and around 200 nm on the other side (see Figure 1).

using the software Fit2D.[24] The sample−detector distance was set to 86.13 mm.

The two-dimensional patterns acquired can provide information about both wide angle (WAXS) and small angle (SAXS) X-ray scattering.

3. RESULTS

3.1. PTT. Infiltration of PTT produces characteristic rod-like entities that can be identified by SEM. In order to visualize the polymer structures, the AAO template was removed by an aqueous 5 wt % sodium hydroxide solution. Well-defined polymer nanorods are obtained (Figure 3), in accordance with the pore sizes of the AAO membrane (Figure 1).

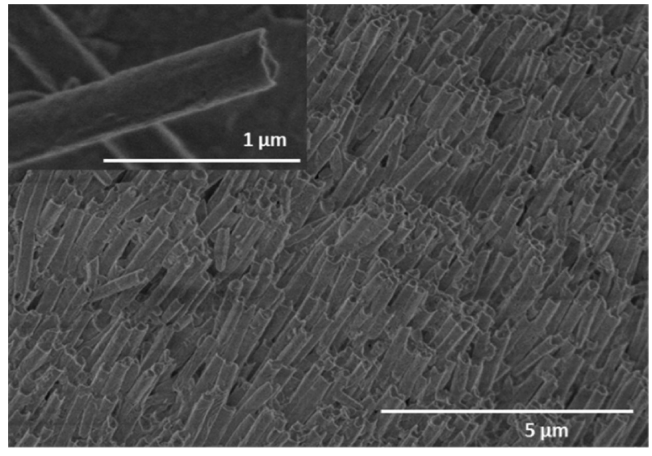

Figure 3. SEM image of PTT nanorods after removing the AAO template. The inset shows a magnification of a nanorod.

Step scan μ-XRD experiments performed for PTT outside the AAO membrane prove that the polymer sample in the bulk is isotropic, as revealed by the WAXS scattering patterns. An example of these patterns is shown in Figure 4a. However, inside the AAO membrane, the polymer shows a clearly oriented pattern (Figure 4b). It is important to remark on the presence of a scattering vertical stripe (see Figure 4a and b) which arises from the sample itself, few millimeters thick, and its alignment (Figure 2). Azimuthal integration of the WAXS region provides 1D intensity profiles as a function of the

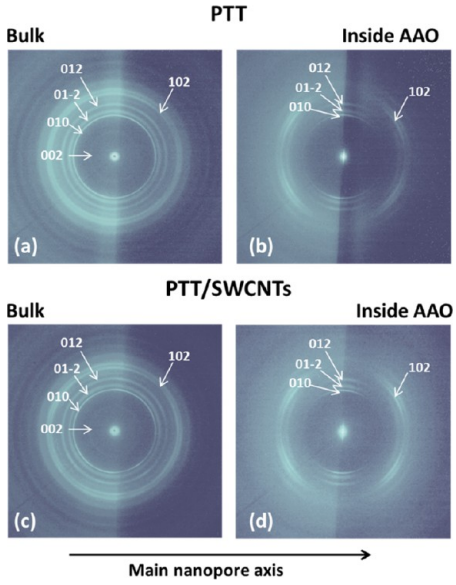

Figure 4. Upper panel: 2D diffraction patterns of PTT outside (a) and inside (b) the AAO membrane. Lower panel: PTT with 0.5 wt % SWCNTs outside (c) and inside (d) the AAO membrane. The equator of the image is aligned with the main pore axis of the AAO membrane.

scattering vector, $q = 4\pi/\lambda(\sin\theta)$, where 2θ is the scattering angle (Figure 5). Integration was performed between −80 and

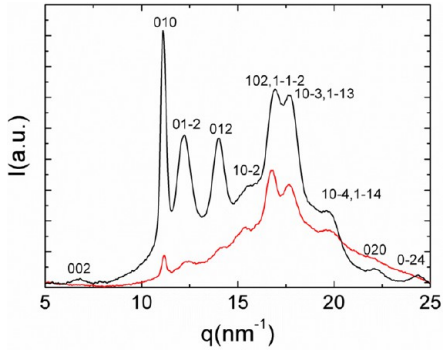

Figure 5. WAXS 1D intensity profile for the bulk PTT film outside the AAO membrane (black) and for PTT inside it (red).

80°, with the equator as the azimuth origin. By integrating in this way, the meridian scattering can be excluded from the angular region of interest. Bragg peaks were indexed following previous works[15,25,26] and by calculating the theoretical Bragg peaks corresponding to a triclinic unit cell with lattice parameters as previously reported.[25] The scattered intensity inside the membrane (Figure 5, red line) is lower than the scattered intensity in bulk PTT (Figure, 5, black line). This might be related to the reduced amount of polymeric material inside the membrane, in conjunction with a decrease in the degree of crystallinity.

Upon indexing, one can see that 0*kl* reflections for infiltrated PTT are concentrated in the meridian (Figure 4b). This implies that the *a*-axis of the PTT crystal unit cell must be oriented along the equator. Previous studies by means of electron diffraction and μ-XRD in bulk PTT have proven the *a*-axis to be the radial growth direction for PTT spherulites.[26,27] Having in mind the setup in our experiments in which the main axis of the AAO pores is parallel to the equator, we can affirm that the growth direction of the PTT crystalline lamellae within the AAO pore coincides with the main axis of the template pores. It is also worth noting that the inner 002 reflection is not detected inside the membrane due to its relatively low intensity and the reduced amount of material present in the pores. In order to characterize the orientation induced by the template confinement, the full width at half-maximum (fwhm) of the 102 reflection was calculated for all the oriented patterns along the scan (Figure 6a). The fwhm values decrease as we move into

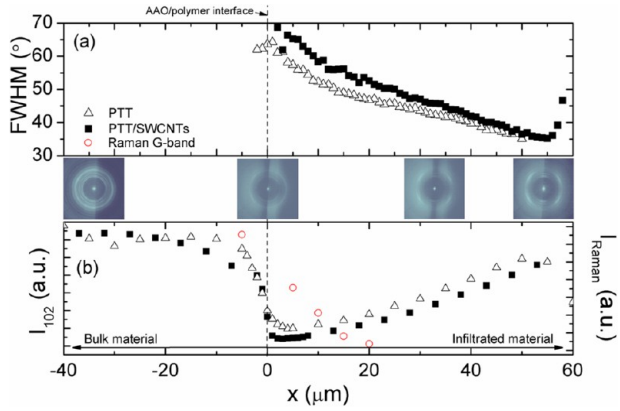

Figure 6. Spatial dependence of (a) the full width at half-maximum (fwhm) of the (102) reflection and (b) peak intensity of the same reflection for neat PTT (■) and for the PTT nanocomposite with 0.5 wt % SWCNTs (△) along with the Raman intensity of the SWCNT G-band (○) (lower plot). $x = 0$ corresponds to the AAO/polymer interface. Some representative 2D diffraction patterns of the PTT/SWCNT nanocomposites for different regions of the sample are presented in between the graphs.

the membrane, indicating an increase in orientation. Figure 6a indicates as well that the AAO membrane has been completely filled with polymer, since the 102 reflection can be detected up to 60 μm deep. This length coincides with the thickness of the AAO membranes.

The spatial dependence of the intensity of the 102 reflection shows a sharp decrease at the AAO/polymer interface and then continuously increases (Figure 6b). This increase confirms that the pores of the AAO membrane, after a thin size-selective layer, widen up to 200 nm on the other side of the template. Thus, the amount of present material is augmented with depth, generating more scattered intensity, which is enhanced as well by the increase in orientation.

Information about the crystalline lamellae distribution can be obtained by zooming in the SAXS region of the 2D patterns. Far from the interface (Figure 7a), SAXS patterns are characteristic of semicrystalline polymers exhibiting the presence of an isotropic ring. This maximum of the scattered SAXS intensity is associated with the long spacing defined as the mean average distance among crystalline lamellae. Azimuthal integration of the SAXS patterns reveals the presence of a maximum in the scattered intensity corresponding to a long spacing value of about $L = 2\pi/q_{max} \approx 10$ nm (Figure 8). Thus, far from the polymer/AAO interface (Figure 7a), the lamellae distribution is isotropic, as one could expect from a bulk polymer sample. As one approaches the polymer/AAO interface, SAXS patterns become anisotropic, exhibiting an excess of scattering at the meridian (Figure 7b). This fact indicates an abundance of crystalline lamellae in an edge-on disposition with respect to the template surface. However, very

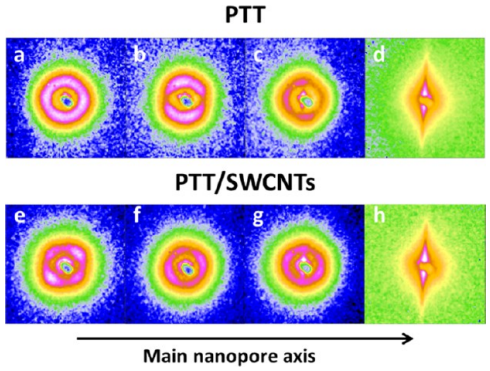

Figure 7. (upper panel) SAXS region of the 2D μ-XRD patterns of the PTT residual film 67 μm (a), 37 μm (b), and 7 μm (c) away from the interface with the membrane. Pattern d corresponds to the interior of the AAO membrane. (lower panel) Similar for the PTT/0.5 wt % SWCNTs composite 100 μm (e), 25 μm (f), and 5 μm (g) away from the interface with the membrane. Pattern h corresponds to the interior of the alumina membrane. The main axis of the AAO pores is aligned with the equator.

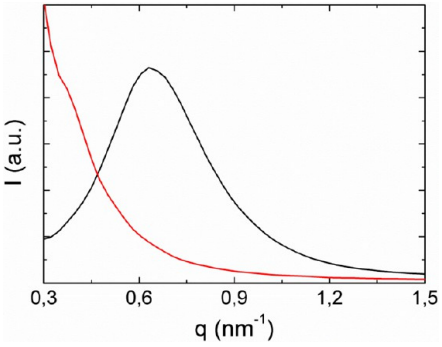

Figure 8. Azimuthally integrated SAXS intensity from Figure 7a for the PTT film outside the AAO membrane (black) and for PTT inside it (red) (from Figure 7d).

close to the interface, SAXS patterns indicate the coexistence of both flat-on and edge-on lamellae. This fact is revealed by the presence of an excess of scattering at the meridian and equator regions (Figure 7c). The appearance of these flat-on lamellae will be addressed in the Discussion section. Inside the membrane, SAXS patterns change dramatically, exhibiting an intense and continuous scattering concentrated on the meridian (Figure 7d). Azimuthal integration of the SAXS patterns in this region reveals the absence of the characteristic maximum of the polymer long-spacing (Figure 8). The shape of the SAXS inside the membrane is related to the scattering of the pores aligned horizontally and perpendicularly to the X-ray beam.

3.2. PTT/SWCNT Composite. The extension of the infiltration within the AAO membrane for the PTT/SWCNT nanocomposites was verified by Raman spectroscopy. Figure 9 shows the Raman spectra of PTT/0.5 wt % SWCNTs collected at different positions of the sample cross section moving from the bulk nanocomposite to inside the AAO membrane. Raman spectra provided evidence of the presence of SWCNTs in the residual nanocomposite film and inside the alumina template by the presence of the characteristic G-band appearing around 1592 cm^{-1} as a double peak. The Raman G-band is associated with the two main tangential modes of SWCNTs.[28] The intensity of the G-band decreases as we scan deeper into the membrane, and even at 20 μm deep, it is possible to detect the

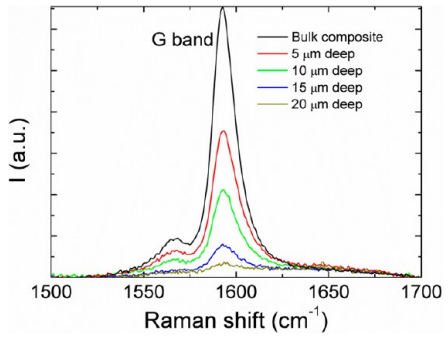

Figure 9. Raman spectra of the PTT/0.5 wt % SWCNT composite at different depths inside the alumina template.

characteristic Raman spectrum coming from the SWCNTs. At deeper positions within the membrane, the Raman signal from the SWCNTs vanishes. Raman intensities of the G-band peak at different depths have been shown in Figure 6b.

WAXS patterns collected for the PTT composite with 0.5 wt % SWCNTs are comparable to those of neat PTT (Figure 4c and d). Outside the template, the WAXS pattern is isotropic, whereas, inside the AAO membrane, it is oriented. There is also a concentration of the 0*kl* reflections in the meridian similarly as for the neat PTT case. The 002 reflection is not observed as in the previous case. The evolution of both the intensity and the fwhm of the 102 reflection for the PTT/SWCNT nanocomposite exhibits a similar dependence as in the case of neat PTT (Figure 6a). This fact will be discussed in the next section.

Regarding SAXS, the analysis of the nanocomposite data is not as straightforward as in the case of PTT. Along the residual film far from the polymer/membrane interface, a characteristic orientation appears, rendering four-point patterns (Figure 7e, lower panel). This most likely appears as a consequence of the templating effect of the SWCNTs over the PTT crystals.[17] As one approaches the AAO interface, SAXS patterns evolve and exhibit an increase in scattered intensity in the equatorial region. This rising intensity indicates a progressive increase of the population of flat-on crystalline lamellae (Figure 7f and g).

4. DISCUSSION

The μ-XRD experiments provide a clear picture of the crystallization behavior of PTT and its nanocomposite with SWCNT in the confined environment associated with the AAO membrane. WAXS results indicate that crystallization of PTT and PTT/SWCNT in these systems mainly starts in the residual film far away from the polymer/membrane interface. This is in agreement with previous studies performed in other semicrystalline polymers infiltrated in AAO membranes.[4,6,7] Considering the spherulitic nature of semicrystalline PTT[26] and the isotropic character of both WAXS (Figure 4a) and SAXS (Figure 7a) patterns, one can infer that isotropic spherulites are formed in the bulk PTT film and grow radially along the *a*-axis direction until they reach the AAO membrane surface. For the PTT/SWCNT nanocomposite, the bulk film exhibits the peculiar template effect of the SWCNT and isotropic spherulites are expected to coexist with kebab-like crystals nucleated in the SWCNT surface.[29] Interestingly enough, at the region close to the AAO interface, an orientation of the crystalline lamellae with an edge-on disposition with respect to the AAO interface is observed, as revealed by the anisotropic SAXS patterns (Figure 7b). This effect suggests an alignment of

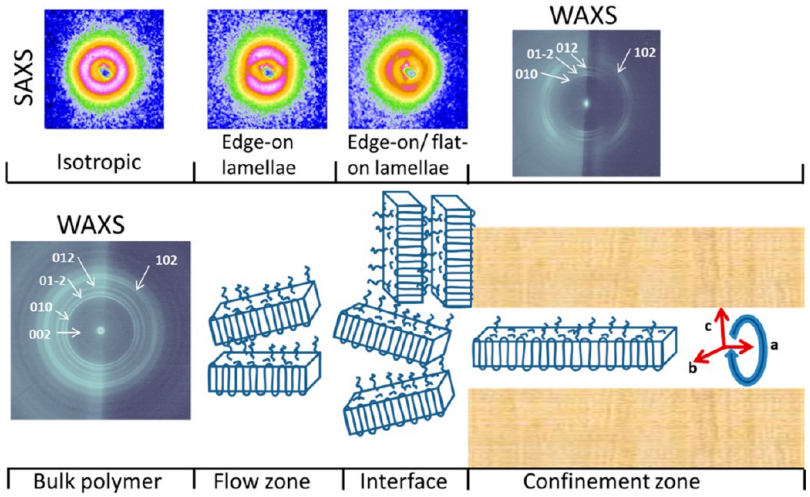

Figure 10. Simplified model describing the different zones affecting the nanostructure of the polymer crystal from left to right: isotropic bulk polymer film, flow induced crystallization zone, and interfacial zone. Inside the pore (confinement zone) a scheme is shown, indicating the three axes of the PTT crystal unit cell. Cylindrical symmetry allows different lamellae orientations around the *a*-axis. The spatial scale is arbitrary.

the polymer crystal *a*-axis with the axis of the membrane nanopores. In a first approach, we can attribute this effect as being due to the elongational flow that probably takes place in the molten state as the polymer chains infiltrate the AAO membrane. It has been fully reported that polymer crystallization under elongational and/or shear flow renders oriented crystals.[29] However, at the polymer/membrane interface, SAXS patterns (Figure 7c) indicate the presence of a significant amount of crystalline lamellae with a flat-on orientation with respect to the AAO interface. Monte Carlo simulations have proven that, when a strong interaction between a polymer melt and a certain wall ("sticky walls") is present, polymer crystallization takes place by favoring flat-on lamellae with polymeric chains perpendicular to the pore wall.[30] In the polymer/AAO case, it is known that the large difference in surface energies between polymer and membrane leads to a strong interaction[2,5] which might even affect both segmental[31] and chain[32] polymer dynamics. Accordingly, we can interpret that at the AAO interface there is a preferential formation of flat-on polymer lamellae induced by the interaction between PTT and the AAO surface. We have already reported this scenario for PVDF.[4] As the polymer crystal front reaches the polymer/membrane interface, only those crystalline lamellae whose *a*-axis is well aligned with the main axis of the membrane nanopores are expected to keep on growing inside the pore. This growth mechanism induces a kinetic selection followed by a quasi-one-dimensional growth along the pores. The fact that the intensity of the 102 reflection increases with pore depth (Figure 6b) might be interpreted as a widening of the pore, since more polymeric material contributes to the scattering after the thin size-selective upper layer. Despite the increase in room available and material involved, the orientation of the crystalline lamella does not significantly change along the pore. In contrast, a progressive improvement with increasing pore depth is clearly observed (Figure 6a). This indicates that kinetic selection originating at the polymer/AAO interface is still dominant within the AAO membrane. The growth of the crystalline lamellae proceeds with the *a*-axis rather parallel to that of the pore. No clear sign of long period is detected at any position within the membrane. This suggests that crystal branching is not likely to occur and the most probable scenario is a thickening of the lamella crystal along the pore. Within the AAO membrane, we can consider that both the "sticky" nature of the polymer/AAO interaction and the kinetic selection of growth directions due to confined geometry add together to favor a preferential disposition of flat-on crystalline lamellae, with respect to the alumina walls. They grow along the polymer crystal *a*-axis parallel to the main axis of the nanopores. However, according to the WAXS patterns, the intrinsic cylindrical symmetry of the system allows a rotation of polymer crystals around the *a*-axis. A schematic model describing the system in accordance with the experimental observations is presented in Figure 10.

Concerning the PTT/SWCNT nanocomposite, outside the AAO membrane, SAXS patterns indicate a slightly preferred flat-on orientation with respect to the membrane (Figure 7a–c). This is compatible with a view in which polymer "kebabs" would be formed over SWCNT "shishes" and these hybrid "shish-kebabs" would tend to orient parallel to the main membrane pore axis. As discussed in the case of neat PTT, we can attribute this effect as being due to an elongational flow forming in the molten state as the polymer chains infiltrate the AAO membrane. This flow favors an orientation of the SWCNTs along the membrane pore axis. Inside the alumina nanopores, it is clear that the orientation of crystalline lamellae is comparable to the case of neat PTT (Figures 4d and 6a). These results are in contrast with other polymer crystallization studies in the presence of SWCNTs[20,33] which provided evidence of their influence as a template for polymer crystallization. Here, we have proven that SWCNTs are present inside the nanopores up to 20 μm deep (Figures 6b and 9). Thus, SWCNTs could have acted as a template, as they do outside the membrane, forming the characteristic shish-kebab structures in which crystal lamellae grow with their chain axis parallel to the SWCNT surface. These lamellae would be edge-on with respect to the pore walls. However, the WAXS patterns for PTT/SWCNT nanocomposites are very similar to those of neat PTT. This means that the influence, if any, of the SWCNTs on the crystallization process inside the AAO template is weak in comparison with the previously described combination of growth kinetic selection and interaction with the alumina walls.

5. CONCLUSIONS

Our experiments have proven that semicrystalline polymer nanorods of PTT and of its nanocomposites with SWCNTs can be obtained upon infiltration of the molten polymer in AAO membranes. X-ray microdiffraction experiments have evidenced different zones where polymer crystals adopt different orientations. While the polymer residual film exhibits isotropic character, edge-on lamellae form upon approaching the polymer/membrane interface. This effect has been explained as being due to the elongational flow that probably forms in the molten state as the polymer chains infiltrate the AAO membrane. For the PTT/SWCNT nanocomposites, this is accompanied by an alignment of the nanotube with the main membrane pore axis. At the interface, edge-on and flat-on crystalline lamellae coexist, appearing as a consequence of the strong interaction between the polymer and the AAO surface. Inside the nanopores, the confined environment induces a kinetic selection of polymer crystals by which only crystalline lamellae growing with their *a*-axis parallel to that of the pore are allowed. For the PTT/SWCNT nanocomposites, this effect, in conjunction with the strong interaction between the polymer and AAO surface, seems to prevail over the templating capacity of the nanotubes and a similar polymer crystal orientation is observed compared to that of neat PTT.

AUTHOR INFORMATION

Corresponding Author

*E-mail: i.fabiani@csic.es.

Notes

The authors declare no competing financial interest.

ACKNOWLEDGMENTS

The authors acknowledge financial support from the MINECO (grants MAT2011-23455, MAT2012-33517, and FPI BES-2010-030074). We thank A. Szymczyk and Z. Rosłaniec for handing over PTT and PTT nanocomposite samples and José David Gómez (ICTP-CSIC) for SEM measurements.

REFERENCES

(1) Martin, C. R. *Science* **1994**, *266*, 1961−1966.
(2) Degennes, P. G. *Rev. Mod. Phys.* **1985**, *57*, 827−863.
(3) Masuda, H.; Fukuda, K. *Science* **1995**, *268*, 1466−1468.
(4) Garcia-Gutierrez, M.-C.; Linares, A.; Hernandez, J. J.; Rueda, D. R.; Ezquerra, T. A.; Poza, P.; Davies, R. J. *Nano Lett.* **2010**, *10*, 1472−1476.
(5) Zhang, M. F.; Dobriyal, P.; Chen, J. T.; Russell, T. P.; Olmo, J.; Merry, A. *Nano Lett.* **2006**, *6*, 1075−1079.
(6) Steinhart, M.; Goering, P.; Dernaika, H.; Prabhukaran, M.; Goesele, U.; Hempel, E.; Thurn-Albrecht, T. *Phys. Rev. Lett.* **2006**, 97.
(7) Wu, H.; Su, Z. H.; Takahara, A. *Soft Matter* **2012**, *8*, 3180−3184.
(8) Duran, H.; Steinhart, M.; Butt, H.-J.; Floudas, G. *Nano Lett.* **2011**, *11*, 1671−1675.
(9) Chen, D.; Zhao, W.; Russell, T. P. *ACS Nano* **2012**, *6*, 1479−1485.
(10) Liu, H. J.; Xu, Y. Z.; Zheng, Z. M.; Liu, D. H. *Biotechnol. J.* **2010**, *5*, 1137−1148.
(11) Lewin, M. In *Handbook of Fiber Chemistry*, 3rd ed.; CRC Press: Boca Raton, FL, 2007.
(12) Wang, Y. Q.; Zhu, H.; Li, B. J. *Opt. Commun.* **2011**, *284*, 3276−3279.
(13) Yu, H.; Liao, D.; Johnston, M. B.; Li, B. *ACS Nano* **2011**, *5*, 2020−2025.
(14) Xing, X.; Zhu, H.; Wang, Y.; Li, B. *Nano Lett.* **2008**, *8*, 2839−2843.
(15) Martin-Fabiani, I.; Rebollar, E.; Perez, S.; Rueda, D. R.; Garcia-Gutierrez, M. C.; Szymczyk, A.; Roslaniec, Z.; Castillejo, M.; Ezquerra, T. A. *Langmuir* **2012**, *28*, 7938−7945.
(16) Rueda, D. R.; Martin-Fabiani, I.; Soccio, M.; Alayo, N.; Perez-Murano, F.; Rebollar, E.; Garcia-Gutierrez, M. C.; Castillejo, M.; Ezquerra, T. A. *J. Appl. Crystallogr.* **2012**, *45*, 1038−1045.
(17) Grow, R. J. In *Carbon Nanotubes: Properties and Applications*, 1st ed.; O'Conell, M. J., Ed.; CRC Press: Boca Raton, FL, 2006; p 187.
(18) Hernandez, J. J.; Garcia-Gutierrez, M. C.; Nogales, A.; Rueda, D. R.; Ezquerra, T. A. *Macromolecules* **2009**, *42*, 4374−4376.
(19) Li, L. Y.; Li, B.; Hood, M. A.; Li, C. Y. *Polymer* **2009**, *50*, 953−965.
(20) Hernandez, J. J.; Garcia-Gutierrez, M.-C.; Rueda, D. R.; Ezquerra, T. A.; Davies, R. J. *Compos. Sci. Technol.* **2012**, *72*, 421−427.
(21) Maiz, J.; Sacristan, J.; Mijangos, C. *Chem. Phys. Lett.* **2010**, *484*, 290−294.
(22) Szymezyk, A.; Senderek, E.; Nastalczyk, J.; RoslanieC, Z. *Eur. Polym. J.* **2008**, *44*, 436−443.
(23) Nogales, A.; Broza, G.; Roslaniec, Z.; Schulte, K.; Sics, I.; Hsiao, B. S.; Sanz, A.; Garcia-Gutierrez, M. C.; Rueda, D. R.; Domingo, C.; Ezquerra, T. A. *Macromolecules* **2004**, *37*, 7669−7672.
(24) Wang, X. S.; Li, X. G.; Yan, D. Y. *Polym. Degrad. Stab.* **2000**, *69*, 361−372.
(25) Wang, B. J.; Li, C. Y.; Hanzlicek, J.; Cheng, S. Z. D.; Geil, P. H.; Grebowicz, J.; Ho, R. M. *Polymer* **2001**, *42*, 7171−7180.
(26) Ho, R. M.; Ke, K. Z.; Chen, M. *Macromolecules* **2000**, *33*, 7529−7537.
(27) Rosenthal, M.; Portale, G.; Burghammer, M.; Bar, G.; Samulski, E. T.; Ivanov, D. A. *Macromolecules* **2012**, *45*, 7454−7460.
(28) Jorio, A.; Pimenta, M. A.; Souza, A. G.; Saito, R.; Dresselhaus, G.; Dresselhaus, M. S. *New J. Phys.* **2003**, *5*, 139.1−139.17.
(29) Garcia-Gutierrez, M. C.; Hernandez, J. J.; Nogales, A.; Pantine, P.; Rueda, D. R.; Ezquerra, T. A. *Macromolecules* **2008**, *41*, 844−851.
(30) Ma, Y.; Hu, W. B.; Hobbs, J.; Reiter, G. *Soft Matter* **2008**, *4*, 540−543.
(31) Martin, J.; Mijangos, C.; Sanz, A.; Ezquerra, T. A.; Nogales, A. *Macromolecules* **2009**, *42*, 5395−5401.
(32) Martin, J.; Krutyeva, M.; Monkenbusch, M.; Arbe, A.; Allgaier, J.; Radulescu, A.; Falus, P.; Maiz, J.; Mijangos, C.; Colmenero, J.; Richter, D. *Phys. Rev. Lett.* **2010**, *104*, 197801.
(33) Chatterjee, T.; Mitchell, C. A.; Hadjiev, V. G.; Krishnamoorti, R. *Macromolecules* **2012**, *45*, 9357−9363.